Quench-Probe Setup as Analyzer of Fractionalized Entanglement Spreading

Nicolas P. Bauer,[1,2,*] Jan Carl Budich,[3,2] Björn Trauzettel,[1,2] and Alessio Calzona[1,2]
[1]Institute of Theoretical Physics and Astrophysics, University of Würzburg, 97074 Würzburg, Germany
[2]Würzburg-Dresden Cluster of Excellence ct.qmat, Germany
[3]Institute of Theoretical Physics, Technische Universität Dresden, 01062 Dresden, Germany

(Received 13 July 2022; accepted 11 April 2023; published 9 May 2023)

We propose a novel spatially inhomogeneous setup for revealing quench-induced fractionalized excitations in entanglement dynamics. In this quench-probe setting, the region undergoing a quantum quench is tunnel coupled to a static region, the probe. Subsequently, the time-dependent entanglement signatures of a tunable subset of excitations propagating to the probe are monitored by energy selectivity. We exemplify the power of this generic approach by identifying a unique dynamical signature associated with the presence of an isolated Majorana zero mode in the postquench Hamiltonian. In this case excitations emitted from the topological part of the system give rise to a fractionalized jump of $\log(2)/2$ in the entanglement entropy of the probe. This dynamical effect is highly sensitive to the localized nature of the Majorana zero mode, but does not require the preparation of a topological initial state.

DOI: 10.1103/PhysRevLett.130.190401

Introduction.—Identifying physical signatures to distinguish and understand phases of matter occurring in nature is a main objective of research in physics. Dynamical approaches probing a system far from thermal equilibrium have become increasingly important. In particular, quantum quenches, i.e., abrupt changes of parameters in the Hamiltonian, have enabled unprecedented insights into structure and dynamics of quantum matter, both in theory [1–3] and experiment [4–8]. A prominent example is provided by the prediction and observation of nonequilibrium topological invariants [9–23] that probe topological properties of matter without requiring the preparation of a topological equilibrium state.

As a powerful and genuinely quantum-mechanical diagnostic tool, the time evolution of entanglement has been widely investigated [1,3,24,25], including dynamical signatures of topology such as protected crossings in the entanglement spectrum [26–30]. In homogeneous integrable systems, the spreading of entanglement after a quench is closely related to the propagation of pairs of entangled quasiparticle excitations with opposite momenta [25,31–33]. For more complex scenarios, involving for example periodic spatial modulations [34] or open systems [35,36], richer entanglement structures related to quench-induced excitations represent a frontier of ongoing research [37–44].

In this Letter, we propose a novel approach for the study of entanglement dynamics in complex systems to selectively analyze a subset of quench-induced excitations. This enables us to identify unique features in the spreading of entanglement, such as fractional jumps of the entanglement entropy (EE). We directly relate their presence to the existence of nontrivial eigenmodes in the postquench Hamiltonian, e.g., topological localized modes. This remarkable capability stems from the hybrid nature of our proposed setup, sketched in Fig. 1(a), where only a part of the system (Q) is quenched while the entanglement is measured in a different (static) region (P), the two being coupled via a (static) separation layer (X). This quench-probe approach provides a new perspective for the analysis of entanglement spreading in highly inhomogeneous systems, paving the way for novel observations that complement the study of (almost) homogeneous setups [13,14,31,32,34,44–47]. Its energy selectivity—due to resonant coupling between regions Q and P—is reminiscent of scanning tunneling spectroscopy.

As a specific case study, we use our approach to analyze the dynamics of the entanglement generated by a localized Majorana zero mode (MZM), hosted by a Kitaev chain (KC) [49–51]. This leads us to the discovery of quantized jumps in the EE of the probe with fractional amplitude

$$\Delta S_P = \frac{\log(2)}{2}. \tag{1}$$

The corresponding trace is provided by the red line in Fig. 1(b). Such a fractional increase, associated with the fractional entropy of a single MZM [52–54], clearly differs from the conventional EE increase $\Delta S_P = \log(2)$ that originates from an ordinary fermionic mode [see the green line in Fig. 1(b)]. The quantization is robust with respect to parameter variations but highly sensitive to the hybridization of two MZMs. These findings, representing a novel dynamical signature associated with a truly isolated MZM, are corroborated by the additional analysis of the mutual information (MI) shared between Q and P [30,36,46],

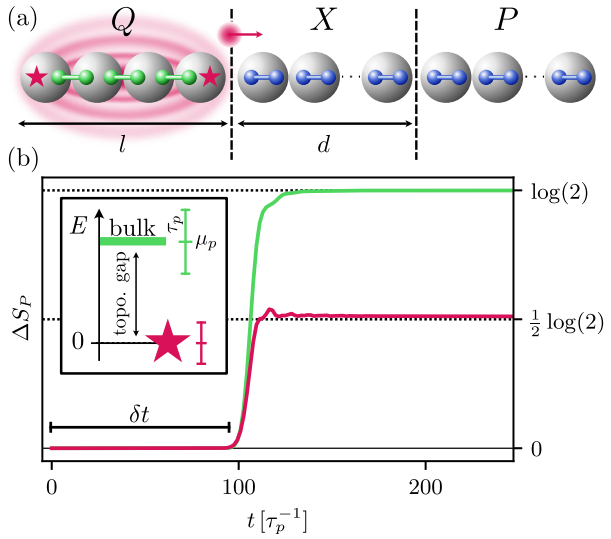

FIG. 1. (a) Hybrid quench-probe setup. A 1D Kitaev chain Q, which undergoes a quantum quench across its topological phase transition, is tunnel coupled at its right end to the trivial regions X and P. Quench-induced excitations are selectively transmitted through X and eventually reach P, whose time-dependent entanglement properties are monitored. (b) Quantized jumps in the entanglement entropy (EE) of the probe. When the latter is selectively coupled to the right Majorana zero mode (MZM) (red star), a robust fractional increase of the EE $\Delta S_P = \log(2)/2$ is observed (red line), which is half of the increase observed when the probe is coupled to the fermionic bulk flatband of the Kitaev chain (green line). A schematic of the energy-selective coupling, allowed by the quench probe approach, is provided in the inset. For our choice of parameters see [48].

which allows us to identify spurious contributions to the EE and highlight the fractional entanglement jumps. Importantly, the observation of this topological signature only requires the postquench Hamiltonian to be topological, while the system can be prepared in a trivial thermal state. The topological nature (and robustness) of an isolated MZM is the origin of the fractional value of ΔS_P. Our setup is applicable to a variety of systems with particular entanglement spreading of either bulk or edge modes. Because of energy selective coupling, we are able to single out the contributions from a subset of modes, if they are separated in energy.

Hybrid quench-probe setup.—We consider the system depicted in Fig. 1(a), consisting of the three parts labeled Q, X, and P. The first one, Q, is the one eventually undergoing a quantum quench. It is an l-site KC described by the Hamiltonian

$$H^Q = \mu \sum_{i=1}^{l} c_i^\dagger c_i + \sum_{i=1}^{l-1} \left(\frac{\tau}{2} c_i^\dagger c_{i+1} + \frac{\Delta}{2} c_i c_{i+1} + \text{H.c.} \right). \quad (2)$$

The operators $c_i^\dagger$ (c_i) create (annihilate) a spinless fermion at site i, μ is the chemical potential, τ the nearest-neighbor hopping amplitude, and Δ the superconducting pairing amplitude. For simplicity, we consider those parameters to be non-negative real numbers. The KC features two different gapped phases, a trivial one for $|\mu| > \tau$ and a topological one for finite Δ and $|\mu| < \tau$. At the topological sweet spot (TSS), i.e., $\tau = \Delta$ and $\mu = 0$, the analysis of H^Q in terms of Majorana operators $c_j = \frac{1}{2}(i\gamma_{2i-1} + \gamma_{2i})$ reveals the presence of two completely isolated MZMs at the two open ends of the chain $[\gamma_1, H^Q] = [\gamma_{2l}, H^Q] = 0$, depicted by red stars in Fig. 1(a). The bulk of the KC at the TSS is described by a flat band at finite energy $E^Q = \tau$. Deviations from the TSS (within the topological phase) imply an exponential leakage of the MZMs into the bulk, whose spectrum acquires then a finite bandwidth $E^Q(k) = \sqrt{[\tau \cos(k) + \mu]^2 + [\Delta \sin(k)]^2}$ [51]. For simplicity, we illustrate the main features of our setup at the TSS. However, the observation of fractional EE is not limited to the TSS as we show below.

The remaining $N - l$ sites of the system are described by a tight-binding Hamiltonian

$$H^{XP} = \sum_{i=l+1}^{N} \mu_p c_i^\dagger c_i + \frac{1}{2} \sum_{j=l+1}^{N-1} \tau_p (c_i^\dagger c_{i+1} + \text{H.c.}), \quad (3)$$

with chemical potential μ_p and hopping amplitude τ_p. The corresponding spectrum reads

$$E^{XP}(k) = \mu_p + \tau_p \cos(k). \quad (4)$$

The first d sites, i.e., the ones between $l < j \leq l + d$, form the separation layer X, while the probe region P consists of the remaining sites with $l + d < j \leq N$. The presence of a finite X allows us to consider regimes in which the probe region P is exclusively affected by quench-induced excitations that propagate ballistically in the chain, filtering out possible contributions to the entanglement associated with the Q-X interface. Regions Q and X are connected via a standard tunneling Hamiltonian

$$H^T = \frac{\tau_t}{2}(c_l^\dagger c_{l+1} + \text{H.c.}) = \frac{\tau_t}{4}[(i\gamma_{2l-1} + \gamma_{2l})c_{l+1} + \text{H.c.}], \quad (5)$$

with coupling strength τ_t.

It is particularly instructive to express fermions in terms of the corresponding Majorana operators. At the TSS, γ_{2l} is an isolated MZM while γ_{2l-1}, together with γ_{2l-2}, belongs to an ordinary fermionic mode of the flat bulk band of the KC. Coupled Majorana operators belonging to the bulk of the KC are depicted by green circles in Fig. 1(a). By properly tuning the parameters of the system, it is thus possible to define two separated regimes. For $|\mu_p| < \tau_p \ll \tau$ the probe is exclusively coupled to the MZM at the right end of the topological KC. By contrast, for $|\mu_p| \sim \tau \gg \tau_p$,

the probe is coupled to the bulk band [55]. A sketch of this energy-selective coupling is provided in the inset of Fig. 1(b). The exploitation of energy and spatial sensitivity, together with the presence of a separation layer X, differentiates our proposal from other quench-probe scenarios, such as the ones discussed in [56–58].

Quench procedure.—The quench of region Q consists in the abrupt change, at $t = 0$, of the parameters $(\mu^i, \tau^i, \Delta^i) \to (\mu^f, \tau^f, \Delta^f)$. We assume the system to be initially prepared in the ground state $|\psi_0\rangle$ of the initial Hamiltonian $H^i = H^Q(\mu^i, \tau^i, \Delta^i) + H^{XP} + H^T$. For $t \geq 0$, the time evolution of the system is instead controlled by the final Hamiltonian $H^f = H^Q(\mu^f, \tau^f, \Delta^f) + H^{XP} + H^T$. With respect to H^f, the state $|\psi_0\rangle$ consists of several quasiparticle excitations, that are emitted in both directions from every site in the quenched region Q. Those counterpropagating quasiparticles are entangled between each other. Their motion is responsible for spreading of correlations and entanglement within the system, bounded by the Lieb-Robinson limit [59]. For a wide range of homogeneous systems, these quasiparticles are produced in uncorrelated pairs, each one consisting of two entangled quasiparticles with opposite momenta [60–64]. The physics is richer in presence of interactions and/or inhomogeneities, which can lead to the presence of quasiparticle multiplets and nontrivial correlations [34,42–44]. When H_f is chosen in the topological regime, our system is spatially inhomogeneous due to the presence of a pair of isolated MZMs. This observation naturally raises the question whether the quasiparticles originating from the MZMs differ from the ones associated with the fermionic bulk of the KC. Our proposed quench-probe setup proves to be particularly effective in providing an affirmative answer to this question.

Entanglement dynamics.—The simplest way to analyze the entanglement properties of P is to compute its EE, defined as

$$S_P(t) = -\mathrm{Tr}\{\rho_P(t)\log[\rho_P(t)]\}. \tag{6}$$

Here, $\rho_P(t)$ is the reduced density matrix of the probe $\rho_P(t) = \mathrm{Tr}_{QX}[\rho(t)]$, whose spectrum can be calculated from the single-particle correlation matrix [65–67]. The time-dependent variation of the EE after a quench to the TSS is shown in Fig. 1(b), where we plot $\Delta S_P(t) = S_P(t) - S_P(0)$ considering a selective coupling either to the isolated MZM (red line) or to the flat fermionic bulk band (green line). After a finite time delay δt, we observe jumps in the EE that eventually reach either the trivial quantized value log(2) (for the coupling to the bulk) or an anomalous fractional value $\log(2)/2$ (for the coupling to the MZM). Consistently with the quasiparticle picture, the time delay satisfies $\delta t \sim d\tau_p^{-1}$. It can be interpreted as the time of flight associated with the excitations, emitted from the last site of Q, that propagates through the d sites of X at the maximum group velocity τ_p [see Eq. (4)]. The lack of a steady linear increase of $\Delta S_P(t)$, typically observed in homogeneous systems [31–33], can be understood in terms of the vanishing group velocity in the bulk of the KC at the TSS. This effectively freezes all the quasiparticles emitted in Q with the only exception of the ones related to γ_{2l-1} and γ_{2l}, which are directly connected to X via H^T. Those quasiparticles are ultimately responsible for the quantized jumps discussed before.

To strengthen the connection between the anomalous fractional jump of the EE and the presence of an isolated MZM, we additionally compute the time-dependent MI shared between the probe P and the quenched region Q. It is defined as

$$I(t) = S_Q(t) + S_P(t) - S_{Q\cup P}(t) \tag{7}$$

and quantifies the total amount of correlations between the two disjoint regions [30,36,46], eliminating spurious contributions to S_P coming from the separation layer X and not from the quenched region Q. The increase of MI $\Delta I(t) = I(t) - I(t_0)$, where $t_0 \lesssim \delta t$ and $I(t_0) \to 0$ for large d [55], is plotted in the inset of Fig. 2 (dashed lines). It shares its main features with ΔS_P. In particular, when the probe is effectively coupled to the fermionic bulk of the KC (dashed lines), ΔI saturates at 2log(2), indicating that P and Q share a conventional fermionic mode [55]. In contrast, when the probe is coupled to the isolated MZM (solid lines), the height of the increase is halved and ΔI saturates at log(2). In the following, we carefully analyze the MZM case.

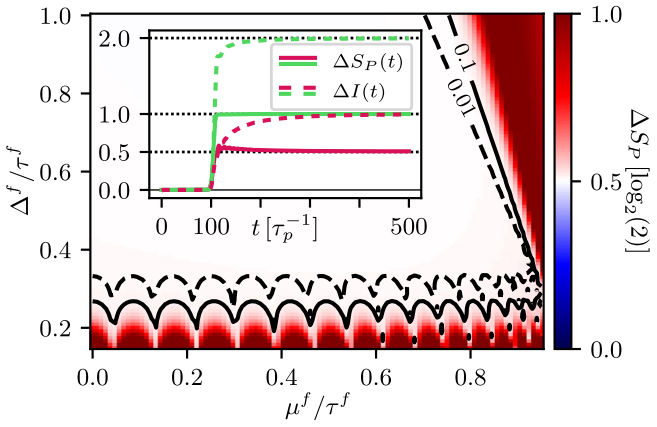

FIG. 2. Fractional quantization of the EE increase as a function of μ^f/τ^f, Δ^f/τ^f ratios. The solid and dotted black lines show the energy splitting of the MZMs in units of $10^{-3}\tau_p$. Inset: quantized jumps in the EE $\Delta S_p(t)$ (solid lines) and MI $\Delta I(t)$ (dashed lines), in units of $\log_2(2)$ for a probe coupled either to the MZM (red lines) or the fermionic bulk modes (green lines). To selectively couple to the MZM (fermionic bulk modes) we choose $\mu_p = 0 (\mu_p = \tau_f)$. For our choice of parameters see [68].

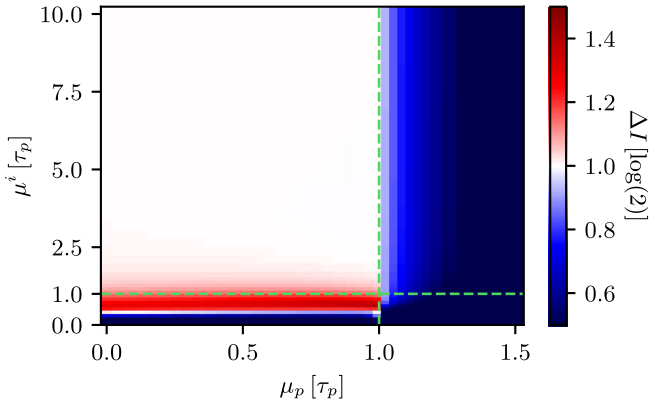

FIG. 3. Quantization of the MI increase. ΔI is plotted as a function of μ^i and μ_p (units τ_p). The dashed horizontal (vertical) line indicates the topological phase transition of the initial Hamiltonian (the transition between a gapless and gapped probe). For our choice of parameters see [70].

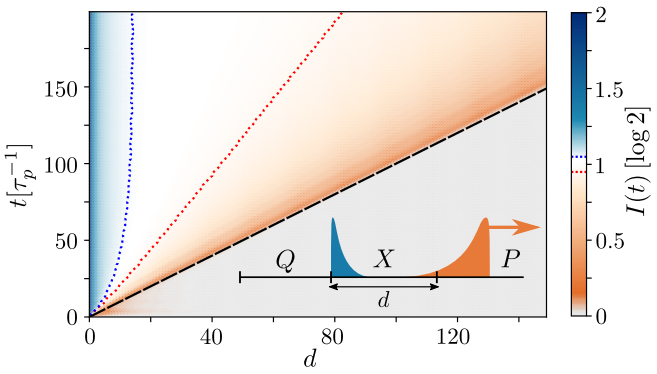

FIG. 4. MI as a function of d and time t. The red(blue)-dotted line corresponds to $I/\log 2 = 0.95$ (1.05). The black-dashed line shows the Lieb-Robinson limit $d = t\tau_p$. The inset shows a sketch of the fixed (blue) and propagating (orange) contributions to the MI. For our choice of parameters see [72].

Anomalous quantization.—After a sufficiently long time t_{sf} and in the large d limit [69], $\Delta I(t_{sf})$ shows a high degree of quantization and robustness. Indeed, as long as the probe is gapless and the initial Hamiltonian features a large trivial gap (such that regions Q and X are initially decoupled), the MI saturates at $\Delta I(t_{sf}) = \log(2)$ without the need of fine-tuning, as shown by the extended white area in Fig. 3. Likewise, no fine-tuning of the tunnel coupling between Q and X is necessary to produce the anomalous quantization signature, as long as it is comparable to τ_p [55]. This anomalous quantization is robust against finite temperature effects and deviations of H^f from the TSS, as can be seen from the large white area in Fig. 2. Away from the TSS, two main effects matter: (i) hybridization of MZMs and (ii) finite bandwidth of the fermionic bulk band. Related to point (i), the hybridization of the MZMs disturbs the saturation of the EE at the fractional value of $\log(2)/2$. This makes sense because hybridized MZMs become regular fermions. If the region Q is, however, chosen long enough such that the hybridization between the MZMs is weak, then the fractional EE can be observed, see Fig. 2. Related to point (ii), as long as the MZMs are energetically decoupled from the bulk, our quench-probe setup allows us to isolate their contribution to the EE by energy selectivity.

As for the robustness at finite temperature, we show that the quantization of the MI is retained even when the system is initialized in a thermal trivial state of H^i at finite temperature T, as long as the latter remains smaller than the topological gap $T \ll \tau^f = \Delta^f$ [55].

Nonequilibrium dynamics.—Our quench-probe setup features another useful knob, i.e., the size d of region X, which can significantly enrich the analysis of the post-quench entanglement dynamics. Indeed, a careful study of $I(t)$ as a function of d (plotted in Fig. 4) reveals the coexistence of a fixed and a propagating component of the correlations contributing to the MI. Let us explain this point by carefully inspecting Fig. 4, from right to left. If the probe region is too far away from Q, the quench-induced excitations have not yet reached P and the MI is basically zero. This explains the large triangular gray area in Fig. 4, which is bounded by the Lieb-Robinson limit $d = t\tau_p$ (black dashed line) [71]. To the left of the Lieb-Robinson line, the MI increases as the probe includes an increasing number of sites entangled with Q (orange region). The MI reaches $I \simeq 0.95\log(2)$ close to the red-dotted line, which we attribute to the propagation of excitations of finite but smaller group velocity than τ_p. To the left of the red-dotted line, the MI features a plateau around the anomalous quantized value of log(2) (white region), the regime described in the previous paragraphs. For small d, i.e., when the probe region starts to include sites close to the Q-X interface, the MI increases again and displays values above log(2) (blue region). Interestingly, the correlations responsible for this additional increase of MI do not propagate within the probe, as shown by the blue-dotted line, corresponding to $I \simeq 1.05\log(2)$, which is asymptotically vertical. Finally, for $d = 0$, the MI reaches the conventional quantized value of $I = 2\log(2)$. At a given (large) time, we can thus identify two groups of sites that are entangled with Q, a propagating one and a fixed one (pinned at the Q-X interface), as sketched in the inset of Fig. 4. The precise and robust quantization of ΔI, shown in Fig. 3, can therefore be understood as the result of a dynamical phenomenon, namely, the separation of the correlations between Q and P into two different components.

Conclusions.—Our quench-probe setup allows us to identify a robust dynamical effect associated with the presence of an isolated MZM, hosted by the postquench topological Hamiltonian. The observation of this effect, consisting of particular fractional quantized jumps in the entanglement properties of the probe, only requires the

preparation of the system in a trivial state. Recent experimental progress shows that it is feasible to measure the second order Renyi entropy by quantum interference [73–75] or randomized measurements [76]. Even though the main focus of our work is put on the von Neumann entropy, we show in the Supplemental Material [55] that all fractional features of the entanglement dynamics of MZMs can also be identified in the second order Renyi entropy. Hence, we are confident that our quench-probe setup can be realized in engineered quantum systems similar to the ones discussed in Refs. [73–76].

This work was supported by the Würzburg-Dresden Cluster of Excellence ct.qmat, EXC2147, project-id 390858490, and the DFG (SPP 1666 and SFB 1170). We thank the Bavarian Ministry of Economic Affairs, Regional Development and Energy for financial support within the High-Tech Agenda Project "Bausteine für das Quanten Computing auf Basis topologischer Materialen".

*nicolas.bauer@physik.uni-wuerzburg.de

[1] C. Gogolin and J. Eisert, Equilibration, thermalisation, and the emergence of statistical mechanics in closed quantum systems, Rep. Prog. Phys. **79**, 056001 (2016).
[2] A. Polkovnikov, K. Sengupta, A. Silva, and M. Vengalattore, Colloquium: Nonequilibrium dynamics of closed interacting quantum systems, Rev. Mod. Phys. **83**, 863 (2011).
[3] F. H. L. Essler and M. Fagotti, Quench dynamics and relaxation in isolated integrable quantum spin chains, J. Stat. Mech. (2016) 064002.
[4] T. Kinoshita, T. Wenger, and D. S. Weiss, A quantum Newton's cradle, Nature (London) **440**, 900 (2006).
[5] M. Gring, M. Kuhnert, T. Langen, T. Kitagawa, B. Rauer, M. Schreitl, I. Mazets, D. A. Smith, E. Demler, and J. Schmiedmayer, Relaxation and prethermalization in an isolated quantum system, Science **337**, 1318 (2012).
[6] M. Cheneau, P. Barmettler, D. Poletti, M. Endres, P. Schauß, T. Fukuhara, C. Gross, I. Bloch, C. Kollath, and S. Kuhr, Light-cone-like spreading of correlations in a quantum many-body system, Nature (London) **481**, 484 (2012).
[7] T. Langen, R. Geiger, M. Kuhnert, B. Rauer, and J. Schmiedmayer, Local emergence of thermal correlations in an isolated quantum many-body system, Nat. Phys. **9**, 640 (2013).
[8] I. Bloch, J. Dalibard, and W. Zwerger, Many-body physics with ultracold gases, Rev. Mod. Phys. **80**, 885 (2008).
[9] P. Hauke, M. Lewenstein, and A. Eckardt, Tomography of Band Insulators from Quench Dynamics, Phys. Rev. Lett. **113**, 045303 (2014).
[10] S. Vajna and B. Dóra, Topological classification of dynamical phase transitions, Phys. Rev. B **91**, 155127 (2015).
[11] J. C. Budich and M. Heyl, Dynamical topological order parameters far from equilibrium, Phys. Rev. B **93**, 085416 (2016).
[12] N. Goldman, J. C. Budich, and P. Zoller, Topological quantum matter with ultracold gases in optical lattices, Nat. Phys. **12**, 639 (2016).
[13] A. Eckardt, Colloquium: Atomic quantum gases in periodically driven optical lattices, Rev. Mod. Phys. **89**, 011004 (2017).
[14] N. R. Cooper, J. Dalibard, and I. B. Spielman, Topological bands for ultracold atoms, Rev. Mod. Phys. **91**, 015005 (2019).
[15] A. Bermudez, D. Patanè, L. Amico, and M. A. Martin-Delgado, Topology-Induced Anomalous Defect Production by Crossing a Quantum Critical Point, Phys. Rev. Lett. **102**, 135702 (2009).
[16] M. D. Caio, N. R. Cooper, and M. J. Bhaseen, Quantum Quenches in Chern Insulators, Phys. Rev. Lett. **115**, 236403 (2015).
[17] Y. Hu, P. Zoller, and J. C. Budich, Dynamical Buildup of a Quantized Hall Response from Nontopological States, Phys. Rev. Lett. **117**, 126803 (2016).
[18] C. Wang, P. Zhang, X. Chen, J. Yu, and H. Zhai, Scheme to Measure the Topological Number of a Chern Insulator from Quench Dynamics, Phys. Rev. Lett. **118**, 185701 (2017).
[19] W. Sun, C.-R. Yi, B.-Z. Wang, W.-W. Zhang, B. C. Sanders, X.-T. Xu, Z.-Y. Wang, J. Schmiedmayer, Y. Deng, X.-J. Liu, S. Chen, and J.-W. Pan, Uncover Topology by Quantum Quench Dynamics, Phys. Rev. Lett. **121**, 250403 (2018).
[20] H. Hu and E. Zhao, Topological Invariants for Quantum Quench Dynamics from Unitary Evolution, Phys. Rev. Lett. **124**, 160402 (2020).
[21] M. McGinley and N. R. Cooper, Topology of One-Dimensional Quantum Systems Out of Equilibrium, Phys. Rev. Lett. **121**, 090401 (2018).
[22] N. Fläschner, D. Vogel, M. Tarnowski, B. S. Rem, D.-S. Lühmann, M. Heyl, J. C. Budich, L. Mathey, K. Sengstock, and C. Weitenberg, Observation of dynamical vortices after quenches in a system with topology, Nat. Phys. **14**, 265 (2017).
[23] J. A. Marks, M. Schüler, and T. P. Devereaux, Dynamical signatures of symmetry protected topology following symmetry breaking, Phys. Rev. Res. **3**, 023137 (2021).
[24] P. Calabrese, F. H. L. Essler, and G. Mussardo, Introduction to 'quantum integrability in out of equilibrium systems', J. Stat. Mech. (2016) 064001.
[25] P. Calabrese, Entanglement spreading in non-equilibrium integrable systems, SciPost Phys. Lect. Notes **20** (2020).
[26] Z. Gong and M. Ueda, Topological Entanglement-Spectrum Crossing in Quench Dynamics, Phys. Rev. Lett. **121**, 250601 (2018).
[27] L. Pastori, S. Barbarino, and J. C. Budich, Signatures of topology in quantum quench dynamics and their interrelation, Phys. Rev. Res. **2**, 033259 (2020).
[28] S. Sayyad, J. Yu, A. G. Grushin, and L. M. Sieberer, Entanglement spectrum crossings reveal non-Hermitian dynamical topology, Phys. Rev. Res. **3**, 033022 (2021).
[29] T. Micallo, V. Vitale, M. Dalmonte, and P. Fromholz, Topological entanglement properties of disconnected partitions in the Su-Schrieffer-Heeger model, SciPost Phys. Core **3**, 12 (2020).
[30] S. Mondal, S. Bandyopadhyay, S. Bhattacharjee, and A. Dutta, Detecting topological phase transitions through entanglement between disconnected partitions in a kitaev chain with long-range interactions, Phys. Rev. B **105**, 085106 (2022).

[31] P. Calabrese and J. Cardy, Evolution of entanglement entropy in one-dimensional systems, J. Stat. Mech. (2005) P04010.

[32] P. Calabrese and J. Cardy, Quantum quenches in $1+1$ dimensional conformal field theories, J. Stat. Mech. (2016) 064003.

[33] H. Kim and D. A. Huse, Ballistic Spreading of Entanglement in a Diffusive Nonintegrable System, Phys. Rev. Lett. **111**, 127205 (2013).

[34] A. Bastianello and P. Calabrese, Spreading of entanglement and correlations after a quench with intertwined quasiparticles, SciPost Phys. **5**, 33 (2018).

[35] V. Alba and F. Carollo, Spreading of correlations in Markovian open quantum systems, Phys. Rev. B **103**, L020302 (2021).

[36] S. Maity, S. Bandyopadhyay, S. Bhattacharjee, and A. Dutta, Growth of mutual information in a quenched one-dimensional open quantum many-body system, Phys. Rev. B **101**, 180301(R) (2020).

[37] V. Alba and F. Heidrich-Meisner, Entanglement spreading after a geometric quench in quantum spin chains, Phys. Rev. B **90**, 075144 (2014).

[38] V. Alba, Entanglement and quantum transport in integrable systems, Phys. Rev. B **97**, 245135 (2018).

[39] B. Bertini, M. Fagotti, L. Piroli, and P. Calabrese, Entanglement evolution and generalised hydrodynamics: Noninteracting systems, J. Phys. A **51**, 39LT01 (2018).

[40] V. Alba, B. Bertini, and M. Fagotti, Entanglement evolution and generalised hydrodynamics: Interacting integrable systems, SciPost Phys. **7**, 5 (2019).

[41] V. Alba, Towards a generalized hydrodynamics description of Rényi entropies in integrable systems, Phys. Rev. B **99**, 045150 (2019).

[42] B. Bertini, E. Tartaglia, and P. Calabrese, Quantum quench in the infinitely repulsive hubbard model: The stationary state, J. Stat. Mech. (2017) 103107.

[43] B. Bertini, E. Tartaglia, and P. Calabrese, Entanglement and diagonal entropies after a quench with no pair structure, J. Stat. Mech. (2018) 063104.

[44] A. Bastianello and M. Collura, Entanglement spreading and quasiparticle picture beyond the pair structure, SciPost Phys. **8**, 45 (2020).

[45] V. Alba and P. Calabrese, Entanglement and thermodynamics after a quantum quench in integrable systems, Proc. Natl. Acad. Sci. U.S.A. **114**, 7947 (2017).

[46] V. Alba and P. Calabrese, Entanglement dynamics after quantum quenches in generic integrable systems, SciPost Phys. **4**, 017 (2018).

[47] G. D. Giulio, R. Arias, and E. Tonni, Entanglement hamiltonians in 1d free lattice models after a global quantum quench, J. Stat. Mech. (2019) 123103.

[48] We choose the following parameter $(\mu^i, \tau^i = \Delta^i = \tau_p) \to (\mu^f = 0, \tau^f = \Delta^f = 11.76\tau_p)$; $N = 500$, $l = 4$, $d = 100$, $t_0 = 10$, $\tau_t = 1\tau_p$.

[49] E. Majorana, Teoria simmetrica dell'elettrone e del positrone, Il Nuovo Cimento **14**, 171 (1937).

[50] A. Y. Kitaev, Unpaired Majorana fermions in quantum wires, Phys. Usp. **44**, 131 (2001).

[51] J. Alicea, New directions in the pursuit of majorana fermions in solid state systems, Rep. Prog. Phys. **75**, 076501 (2012).

[52] E. Sela, Y. Oreg, S. Plugge, N. Hartman, S. Lüscher, and J. Folk, Detecting the Universal Fractional Entropy of Majorana Zero Modes, Phys. Rev. Lett. **123**, 147702 (2019).

[53] S. Smirnov, Majorana tunneling entropy, Phys. Rev. B **92**, 195312 (2015).

[54] J. F. Silva, Luis G. G. V. Dias da Silva, and E. Vernek, Robustness of the Kondo effect in a quantum dot coupled to Majorana zero modes, Phys. Rev. B **101**, 075428 (2020).

[55] See Supplemental Material at http://link.aps.org/supplemental/10.1103/PhysRevLett.130.190401 which includes Refs. [67,73–79] and contains (i) A discussion about the origin of the fractional entanglement signature in the mutual information; (ii) An analysis of the initial entanglement; (iii) A study of the dispersion of the entanglement quasiparticles in the X region; (iv) An extended analysis of the robustness of the fractional entanglement signature; (v) An analysis of the fractional entanglement signature using the experimental relevant second order Rényi entropy.

[56] A. Calzona, F. M. Gambetta, F. Cavaliere, M. Carrega, and M. Sassetti, Quench-induced entanglement and relaxation dynamics in Luttinger liquids, Phys. Rev. B **96**, 085423 (2017).

[57] A. Calzona, F. M. Gambetta, M. Carrega, F. Cavaliere, T. Schmidt, and M. Sassetti, Universal scaling of quench-induced correlations in a one-dimensional channel at finite temperature, SciPost Phys. **4**, 023 (2018).

[58] P. Ruggiero, P. Calabrese, L. Foini, and T. Giamarchi, Quenches in initially coupled Tomonaga-Luttinger liquids: A conformal field theory approach, SciPost Phys. **11**, 055 (2021).

[59] E. H. Lieb and D. W. Robinson, The finite group velocity of quantum spin systems, Commun. Math. Phys. **28**, 251 (1972).

[60] M. A. Cazalilla, A. Iucci, and M.-C. Chung, Thermalization and quantum correlations in exactly solvable models, Phys. Rev. E **85**, 011133 (2012).

[61] D. Schuricht and F. H. L. Essler, Dynamics in the Ising field theory after a quantum quench, J. Stat. Mech. (2012) P04017.

[62] M. A. Cazalilla, Effect of Suddenly Turning on Interactions in the Luttinger Model, Phys. Rev. Lett. **97**, 156403 (2006).

[63] J. De Nardis, B. Wouters, M. Brockmann, and J.-S. Caux, Solution for an interaction quench in the Lieb-Liniger Bose gas, Phys. Rev. A **89**, 033601 (2014).

[64] M. Brockmann, J. D. Nardis, B. Wouters, and J.-S. Caux, Néel-XXZ state overlaps: Odd particle numbers and Lieb–Liniger scaling limit, J. Phys. A **47**, 345003 (2014).

[65] I. Peschel, Calculation of reduced density matrices from correlation functions, J. Phys. A **36**, L205 (2003).

[66] I. Peschel and V. Eisler, Reduced density matrices and entanglement entropy in free lattice models, J. Phys. A **42**, 504003 (2009).

[67] G. Vidal, J. I. Latorre, E. Rico, and A. Kitaev, Entanglement in Quantum Critical Phenomena, Phys. Rev. Lett. **90**, 227902 (2003).

[68] The parameters used in the main figure are $(\mu^i = 20\tau_p, \tau^i = \Delta^i = \tau_p, \tau^f = 20\tau_p)$; $N = 700$, $l = 35$, $d = 100$, $t_{sf} = 1100\tau_p^{-1}$, $\tau_t = 1\tau_p$. In the inset our parameter choice is $(\mu^i, \tau^i = \Delta^i = \tau_p) \to (\mu^f = 0, \tau^f = \Delta^f = 20\tau_p)$; $N = 500$, $l = 4$, $d = 100$, $t_0 = 10\tau_p^{-1}$, $\tau_t = 1\tau_p$. Note, for ease of computing we use $l = 4$ if we quench to the TSS where the MZMs are perfectly localized at the edges. For quenches away from the TSS we need to increase l to avoid hybridization.

[69] Note that the maximum time that can be actually studied is limited by the finite number of sites N because we want to avoid a signal that stems from the reflections of quasiparticles at the right end of the region P. The dependence of the signal on d, the length of the region X, is further discussed in the description of Fig. 4.

[70] The parameters used in the figure are $(\mu^i, \tau^i = \Delta^i = \tau_p) \to (\mu^f = 0, \tau^f = \Delta^f = 20\tau_p)$; $N = 2000$, $l = 4$, $d = 100$, $t_0 = 80\tau_p^{-1}$, $t_{sf} = 3000\tau_p^{-1}$, $\tau_t = 1\tau_p$.

[71] The small deviations from $I = 0$, which can be observed below the dashed line for small d, are a consequence of the nonlocal nature of the MI.

[72] We choose the following parameter $(\mu^i, \tau^i = \Delta^i = \tau_p) \to (\mu^f = 0, \tau^f = \Delta^f = 11.76\tau_p)$; $N = 350$, $l = 100$, $d = 100$, $t_0 = 10$, $\tau_t = 1\tau_p$.

[73] R. Islam, R. Ma, P. M. Preiss, M. Eric Tai, A. Lukin, M. Rispoli, and M. Greiner, Measuring entanglement entropy in a quantum many-body system, Nature (London) **528**, 77 (2015).

[74] A. M. Kaufman, M. E. Tai, A. Lukin, M. Rispoli, R. Schittko, P. M. Preiss, and M. Greiner, Quantum thermalization through entanglement in an isolated many-body system, Science **353**, 794 (2016).

[75] A. Lukin, M. Rispoli, R. Schittko, M. E. Tai, A. M. Kaufman, S. Choi, V. Khemani, J. Léonard, and M. Greiner, Probing entanglement in a many-body–localized system, Science **364**, 256 (2019).

[76] T. Brydges, A. Elben, P. Jurcevic, B. Vermersch, C. Maier, B. P. Lanyon, P. Zoller, R. Blatt, and C. F. Roos, Probing Rényi entanglement entropy via randomized measurements, Science **364**, 260 (2019).

[77] L. Levy and M. Goldstein, Entanglement and disordered-enhanced topological phase in the Kitaev chain, Universe **5**, 33 (2019).

[78] P. Calabrese and J. Cardy, Entanglement entropy and quantum field theory, J. Stat. Mech. (2004) P06002.

[79] C. Holzhey, F. Larsen, and F. Wilczek, Geometric and renormalized entropy in conformal field theory, Nucl. Phys. **B424**, 443 (1994).